IEEE Access
Multidisciplinary | Rapid Review | Open Access Journal

Received 21 April 2023, accepted 29 April 2023, date of publication 2 May 2023, date of current version 9 May 2023.

Digital Object Identifier 10.1109/ACCESS.2023.3272569

RESEARCH ARTICLE

Plasma-Based Intelligent Reflecting Surface for Beam-Steering and Polarization Conversion

MIRKO MAGAROTTO, (Member, IEEE), LUCA SCHENATO, (Member, IEEE), MARCO SANTAGIUSTINA, (Member, IEEE), ANDREA GALTAROSSA, (Fellow, IEEE), AND ANTONIO-DANIELE CAPOBIANCO, (Member, IEEE)

Department of Information Engineering, University of Padua, 35122 Padua, Italy
National Inter-University Consortium for Telecommunications (CNIT), 43100 Parma, Italy

Corresponding author: Mirko Magarotto (mirko.magarotto@unipd.it)

This work was supported in part by the European Union under the Italian National Recovery and Resilience Plan (NRRP) of NextGenerationEU partnership on "Telecommunications of the Future" through the Program RESTART under Grant PE00000001.

ABSTRACT The design of a reflective surface operated in the GHz range is proposed to enable beam-steering and polarization conversion simultaneously. The concept presented in this work relies on plasma-based Intelligent Reflecting Surfaces (IRS) in which the plasma is magnetized. Plasma-based IRSs have been introduced recently and consist of rectangular plasma discharges placed on top of a metallic ground plane. The reflected signal can be reconfigured electronically by varying the plasma parameters (e.g., density). First, a theoretical model is exploited to evaluate the capability of a plasma-based IRS to implement beam-steering and polarization conversion simultaneously. Second, the preliminary design of two plasma-based IRSs is presented to combine beam-steering with 1) cross-polarization or 2) linear-to-circular polarization conversion. According to the numerical results, the proposed concepts are feasible assuming the plasma density can be reconfigured in the range 4.9×10^{17}-13.7×10^{17} m^{-3} and the intensity of the magnetostatic field in the range 60-183 mT; these values are consistent with the plasma technology at the state-of-the-art. The operation frequency is 10 GHz, and the bandwidth is between 0.5-0.8 GHz for the two plasma-based IRSs presented in this work.

INDEX TERMS Gaseous plasma antennas, intelligent reflecting surfaces, beam-steering, polarization conversion, linear-to-circular, cross-polarisation.

I. INTRODUCTION

Intelligent Reflecting Surfaces (IRSs) [1] are planar structures capable of controlling a reflected signal in terms of amplitude, phase, polarisation, and frequency by tuning the electromagnetic (EM) properties of the surface [2]. IRSs have been proposed to optimise the medium between the transmitter and the receiver antennas by enabling the smart reconfigurability of the radiation environment [3]. IRSs are usually implemented via phased arrays or metasurfaces [4]. Specifically, an IRS comprises many unit cells embedding active elements (e.g., PIN or varactor diodes) [5]. Thus, each unit cell can be controlled independently to change the reflected signal's amplitude and phase, enabling fine beam shaping [6].

In this framework, much effort has been devoted to tunable metasurfaces whose operation status can be dynamically controlled [7], [8], [9], [10]. Considering the variety of potential applications, the necessity to develop multifunctional devices is topical [11]. For example, combining beam-steering and polarization conversion in one single device would be paramount in networks that rely on circularly polarized signals such as satellite communications [12]. Several metasurfaces operated in the optical frequency range have been proposed to enable efficient polarization conversion while ensuring complete phase control over the reflected fields [13]. Nonetheless, it is more challenging to achieve such multifunctionality in devices operating in the GHz range [14]. Transmittarrays have been proposed to combine

The associate editor coordinating the review of this manuscript and approving it for publication was Qi Luo.

beam-steering and polarization manipulation [15]. To this end, dedicated unit cells have been developed with an active side that radiates EM waves at an appropriate polarization, an integrated phase shifter, and a passive side used as a receiver [16]. In [11], a beam-steering capability of ±60° is combined with the possibility to select between several linear polarization (LP) and circular polarization (CP) modes. In [17], similar beam-steering capabilities are demonstrated for a CP signal in Ka-band. Another option is to use phased arrays. Nonetheless, effective solutions are available only in the 100 GHz frequency range [18]. The most critical architecture to implement multifunctional capabilities is the reflective surface [19]. In literature, solutions are proposed to select between different functionalities (e.g., beam-steering or polarization control), not to enable them simultaneously [14], [20]. On the other hand, designs are proposed to combine beam-steering and polarization conversion at the expense of the reconfigurability [21], [22], [23].

Gaseous Plasma Antennas (GPAs) [24] constitute another class of devices that allows dynamic control of their operation status [25], [26]. In these systems, the transmission and reception of EM waves are conveyed through an ionised gas, namely plasma [27]. Controlling the electrical power coupled to the plasma enables reconfiguring parameters as the density [28], [29] which, in turn, significantly affect the EM response of a GPA [30], [31]. This feature can be exploited to reconfigure the radiation pattern [32], [33] and the operation frequency [34], [35] of these devices. Notably, the possibility of controlling beam-steering and polarization via GPAs has been demonstrated in the literature. Phased arrays have been proposed to reconfigure the radiation pattern via an appropriate digital switching sequence while ensuring CP [36]. Surfaces working in transmission [37] and reflection [38] mode have been studied to enable polarization conversion in terms of LP and CP. More recently, plasma-based IRSs with beam-steering [39] and polarization conversion [40] capabilities have been proposed. A plasma-based IRS consists of plasma discharges of rectangular shape placed on top of a metallic ground plane, and the reflected signal is reconfigured, controlling the plasma parameters electronically [39]. Notably, polarization conversion is feasible using a magnetised plasma [40].

To the author's knowledge, this is the first time a reflective surface operated in the GHz range is proposed to enable beam-steering and polarization conversion simultaneously. A preliminary design has been elaborated via a theoretical/numerical approach; it relies on a plasma-based IRS in which the plasma is magnetized. An operation frequency $f = 10$ GHz has been assumed [41], [42]. This value is within the range of interest for communications beyond-5G (i.e., from sub-6 up to 300 GHz [43]). Section II outlines the theoretical and numerical models. In Section III, the theoretical model is exploited to analyse the capability of a plasma-based IRS to combine beam-steering with polarization conversion. In Section IV, the plasma elements constituting the IRS are analysed numerically. In Section V, the preliminary design of two plasma-based IRSs enabling beam-steering and 1) cross-polarization conversion or 2) LP-to-CP conversion is discussed. Finally, conclusions are drawn, and future works are outlined in Section VI.

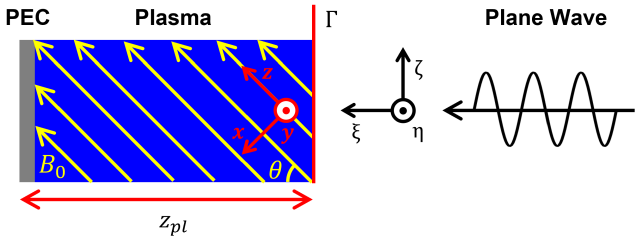

FIGURE 1. Schematic of the plasma slab handled by the theoretical model.

II. METHODOLOGY

The methodology to study the reflection of an EM wave through a plasma slab is outlined in the following. For a more detailed description of the theoretical and numerical models, the reader is referred to [39] and [40].

The response of a magnetized plasma to an impinging EM wave depends on the following parameters [40]

$$\omega_p = \sqrt{\frac{q^2 n_e}{m\varepsilon_0}}, \qquad \omega_c = \frac{qB_0}{m}, \qquad \nu = n_0 K(T_e) \tag{1}$$

where ω_p is the plasma frequency in rad/s, ω_c is the cyclotron frequency in rad/s, and ν is the collision frequency in Hz. Specifically, q is the elementary charge, m is the electron mass, ε_0 is the vacuum permittivity, n_e is the plasma density in m^{-3}, B_0 is the intensity of the magnetostatic field in T, n_0 is the neutral gas density, and K is a rate coefficient that depends on the electron temperature T_e [39]. Provided that ω_p depends on n_e and ω_c on B_0, it is possible to reconfigure the EM response of the plasma acting on two macroscopic parameters. The power spent to sustain the discharge drives n_e [34], while B_0 can be controlled relying on electromagnets [44]. On the other hand, ν is directly related to Ohmic losses occurring within the plasma medium and is proportional to n_0 [39]. The neutral gas pressure p_0 is more often used to characterize plasma discharges rather than n_0 [31], [34].

In the theoretical model, a linearly polarized plane wave is assumed to impact normally a homogeneous plasma slab of thickness z_{pl} placed on top of an infinite ground plane realized in a perfect electric conductor (PEC) (see Fig. 1). The incident wave propagates along the ξ-axis, normally to the ground plane, and forms an angle θ with the uniform magnetostatic field vector. The reflected field reads [40]

$$\boldsymbol{E}_r = \Gamma^+ \boldsymbol{E}_i^+ + \Gamma^- \boldsymbol{E}_i^- \tag{2}$$

where $\boldsymbol{E}_i$ and $\boldsymbol{E}_r$ are complex electric field vectors describing the incident and reflected waves, respectively, and Γ is the reflection coefficient. Superscripts refer to the components of

the incident wave that couple to the two propagation modes that occur within a magnetized plasma referred to as *mode* + and *mode* −, respectively [45]. The fields and the reflection coefficients associated with each mode can be computed according to the methodology described in [40]. Notably, the reliability of the theoretical model has been assessed in [39] and [40] verifying its results against numerical predictions. Given the value of $\boldsymbol{E}_r$, the reflected wave can be analysed in terms of phase front and polarisation. In particular, cross-polarization conversion is studied via the polarisation conversion ratio PCR, which quantifies the amount of power transferred from the incident field to its cross-polarized direction [40]. LP-to-CP conversion is analysed via the axial ratio AR which is defined as the ratio between the major and the minor axes of a generic polarisation ellipse; conventionally, CP is achieved for AR $\leq$ 3 dB [46].

Numerical simulations are performed with the commercial software CST microwave Studio®; two types of analyses have been accomplished. First, the reflection of a linearly polarized plane wave on a $L_{pl} \times L_{pl}$ square plasma element, placed on top of a $L \times L$ ground plane, is studied relying on Floquet boundary conditions [39]. This is propaedeutic to the second analysis, in which the design of an array of plasma elements is presented to combine beam-steering and polarization-conversion. The latter analysis is performed relying on open boundary conditions. Beam-steering is analysed in terms of the radar cross section (RCS) diagrams [39].

Finally, in Appendix A plasma sources at the state of the art [47], [48] have been characterized experimentally to prove that the plasma parameters adopted in this paper are compatible with the current technology.

III. THEORETICAL ANALYSIS

The theoretical model outlined in Section II has been exploited to investigate the capability of a plasma-based IRS to combine beam-steering with cross-polarisation or LP-to-CP conversion, respectively.

A. CROSS-POLARISATION CONVERSION

The considered plasma slab has thickness $z_{pl} = 36$ mm, namely 1.2λ at the operation frequency $f = 10$ GHz. Provided the results in terms of cross-polarisation conversion reported in [40], the magnetostatic field is assumed aligned along the ξ-axis, namely $\theta = 0°$. The neutral gas pressure is $p_0 = 0.4$ mbar provided that this value is consistent with the discharge technology at the state-of-the-art [31]; consequently, the collision frequency is $\nu = 3.1 \times 10^8$ Hz. For the sake of simplicity, the incident wave is assumed polarized along the η-axis, parallel to the ground plane. Thus, the following reflection coefficients

$$\begin{cases} \Gamma_{\eta\eta} = E_{\eta,r}/E_{\eta,i} \\ \Gamma_{\zeta\eta} = E_{\zeta,r}/E_{\eta,i} \end{cases} \tag{3}$$

are sufficient to describe the reflection process. Hence, the PCR quantifies the power transferred to the ζ-axis and reads

$$\text{PCR} = \frac{|\Gamma_{\zeta\eta}|^2}{|\Gamma_{\zeta\eta}|^2 + |\Gamma_{\eta\eta}|^2}. \tag{4}$$

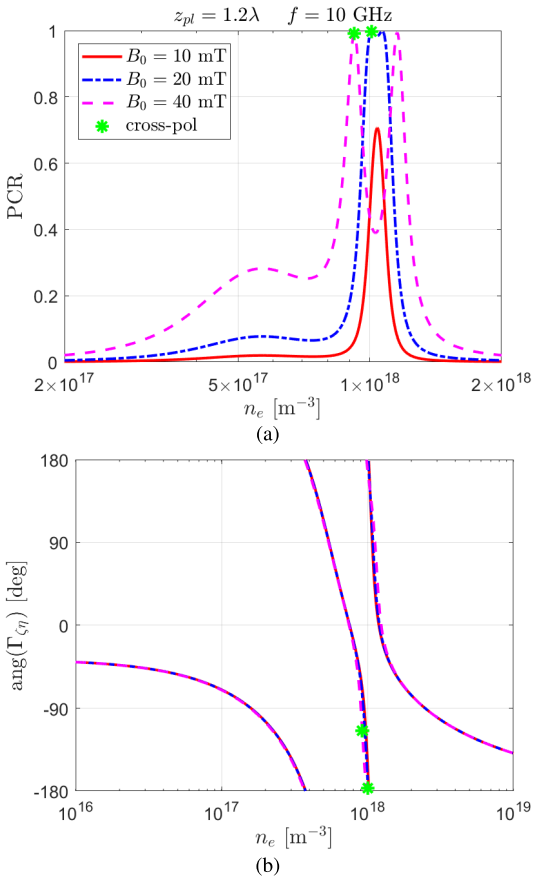

FIGURE 2. (a) Polarisation conversion ratio PCR, and (b) phase of the reflection coefficient $\Gamma_{\zeta\eta}$ in function of the plasma density n_e. Comparison among different values of the magnetostatic field B_0. Configurations in which cross-polarisation conversion occurs are highlighted. Incident field aligned with η-axis, $\theta = 0°$, $\nu = 3.1 \times 10^8$ Hz.

In Fig. 2, PCR and the phase of $\Gamma_{\zeta\eta}$ are depicted in function of the plasma density n_e for three different values of B_0. Interestingly, there is a threshold value of B_0, between 10 mT and 20 mT, above which PCR $\approx$ 1 for at least one value of n_e. In these points, indicated with green stars in Fig. 2, the cross-polarisation conversion occurs; namely, the reflected wave is practically polarized along the ζ-axis. At the same time, the phase of the reflected wave, namely ang($\Gamma_{\zeta\eta}$), is mildly affected by the value of B_0 but depends on n_e. It is therefore possible to find combinations of B_0 and n_e that allow to reconfigure ang($\Gamma_{\zeta\eta}$) over 360° while maintaining PCR $\approx$ 1 and $|\Gamma_{\zeta\eta}| > -1$ dB (see Fig. 3). Consistently with the results reported in Fig. 2, progressively lower values of n_e are required to obtain cross-polarisation conversion as B_0 increases. At the same time, assuming n_e can be controlled in the range $2 \times 10^{17} - 1 \times 10^{18}$ m^{-3} and B_0 in the range 20 − 190 mT, complete control of the phase of the reflected wave is ensured. Being these values compatible with

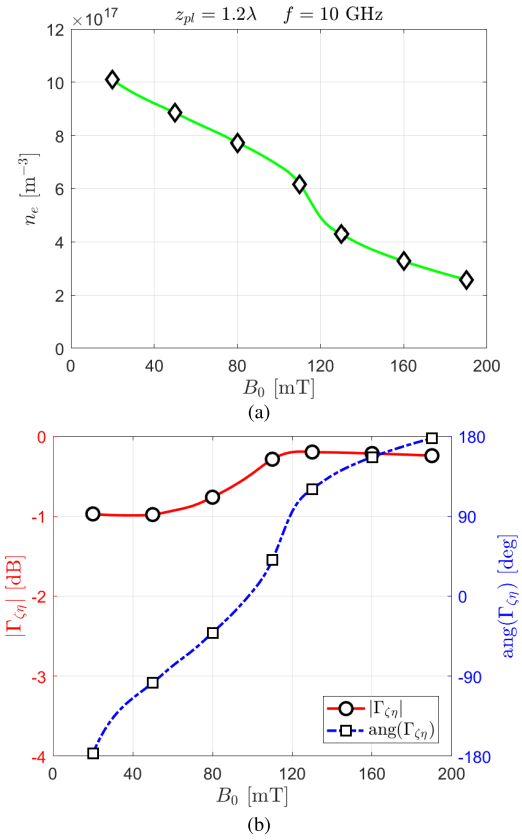

FIGURE 3. (a) Plasma density n_e to maximize the cross-polarisation conversion, and (b) amplitude and phase of the reflection coefficient $\Gamma_{\zeta\eta}$ in the function of the magnetostatic field B_0. Incident field aligned with the η-axis, $\theta = 0°$, $\nu = 3.1 \times 10^8$ Hz.

the plasma technology at the state-of-the-art [31], [44], it is proven that plasma-based IRSs are a promising technology to combine beam-steering and cross-polarisation conversion. Moreover, considering that ang($\Gamma_{\zeta\eta}$) is reconfigurable over 360°, both continuous and discrete control strategies can be implemented to steer the reflected beam [7].

Results can be interpreted considering that the two propagation modes occurring for $\theta = 0°$ are L-waves and R-waves, respectively [45]. The two waves propagate along the ξ-axis; they are left-handed and right-handed CP, respectively. Provided that the refractive index of the two modes is different [45], the longer the path travelled by a wave within the plasma slab, the larger the Faraday rotation effect [40]. Specifically, n_e and B_0 affect the distance required to rotate the polarisation direction of 90° [40]. The combinations n_e-B_0 reported in Fig. 3(a) are exactly the ones for which a plasma slab of thickness z_{pl} is required to obtain cross-polarisation conversion. At the same time, different couples n_e-B_0 provide diverse values of the phase of the reflected wave.

B. LINEAR-TO-CIRCULAR CONVERSION

A plasma slab of thickness $z_{pl} = 24$ mm is considered to study the combination of beam-steering and LP-to-CP conversion. At the operation frequency $f = 10$ GHz, the

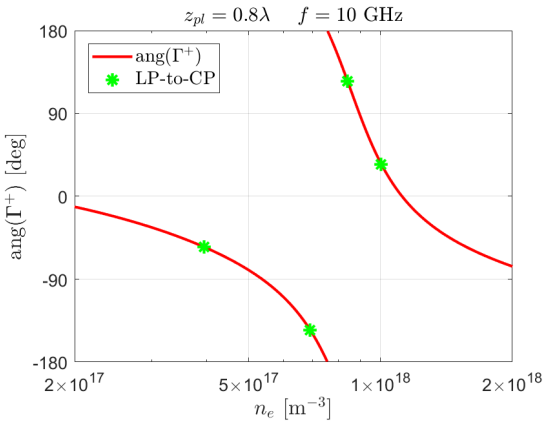

FIGURE 4. Phase of the reflection coefficient Γ^+ in function of the plasma density n_e. Four states to implement LP-to-CP conversion maintaining a phase difference of ±90° are highlighted. Incident field has equal components along η-axis and ζ-axis, $\theta = 90°$, $\nu = 3.1 \times 10^8$ Hz.

TABLE 1. States to implement LP-to-CP conversion maintaining a phase difference of ±90° according to the theoretical model (see Fig. 4).

n_e [10^{17} m^{-3}]	B_0 [mT]	ang(Γ^+) [deg]	$\lvert\Gamma^+\rvert$ [dB]	AR [dB]
10.0	90	35	−0.3	0.72
8.4	85	125	−0.4	0.91
6.9	100	−145	−0.2	0.56
4.0	190	−55	−0.1	1.17

thickness is equivalent to 0.8λ. According to the results of [40], the magnetostatic field is aligned along the ζ-axis, namely $\theta = 90°$, and the incident wave has equal components along the η-axis and the ζ-axis. This configuration produces a reflected beam that is left-handed CP [40]. If right-handed CP is required, it is necessary to align the magnetostatic field along the η-axis instead of the ζ-axis, maintaining $\theta = 90°$ [40]. Regarding the neutral gas, $p_0 = 0.4$ mbar and $\nu = 3.1 \times 10^8$ Hz.

In the case of $\theta = 90°$, the two propagation modes are associated with O-waves and X-waves, respectively [45]. The two modes are orthogonal, namely the component $E_{\zeta,i}$ couples to the O-wave and $E_{\eta,i}$ to the X-wave [40]:

$$\begin{cases} \Gamma^+ = E_{\zeta,r}/E_{\zeta,i} \\ \Gamma^- = E_{\eta,r}/E_{\eta,i} \end{cases} . \tag{5}$$

Interestingly, the propagation along the ζ-axis is parallel to the magnetostatic field, so Γ^+ is independent of the B_0 value [40]. Generally speaking, CP is achieved if $E_{\zeta,r}$ and $E_{\eta,r}$ (i.e., Γ^+ and Γ^-) are 90° out of phase [46]. In that case, implementing beam-steering can be achieved simply via Γ^+ provided the phase difference between $E_{\zeta,r}$ and $E_{\eta,r}$ is fixed. The phase of Γ^+ is depicted in Fig. 4 as a function of n_e. The four states highlighted with green stars present a phase difference of ±90° among each other. Given that B_0 is properly selected (see Table 1), these four states enable

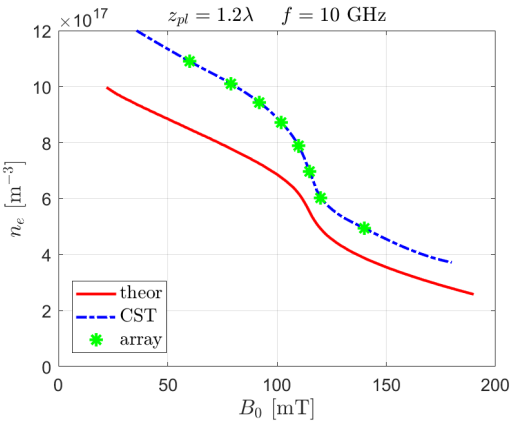

FIGURE 5. Plasma density n_e to maximize the cross-polarisation conversion in function of the magnetostatic field B_0. Theoretical ("theor") and Floquet ("CST") predictions were compared. Eight states to implement beam-steering are highlighted. Incident field aligned with η-axis, $\theta = 0°$, $\nu = 3.1 \times 10^8$ Hz.

TABLE 2. States to implement cross-polarisation conversion and beam-steering according to the Floquet analysis (see Fig. 5).

n_e [10^{17} m^{-3}]	B_0 [mT]	ang($\Gamma_{\zeta\eta}$) [deg]	$\lvert\Gamma_{\zeta\eta}\rvert$ [dB]	PCR [dB]
10.9	60	−60.0	−1.0	−0.09
10.1	79	−28.7	−0.9	−0.17
9.4	92	2.5	−0.7	−0.15
8.7	102	33.8	−0.5	−0.10
7.9	110	65.0	−0.3	−0.09
7.0	115	96.3	−0.2	−0.03
6.0	120	127.5	−0.2	−0.03
4.9	140	158.8	−0.3	−0.12

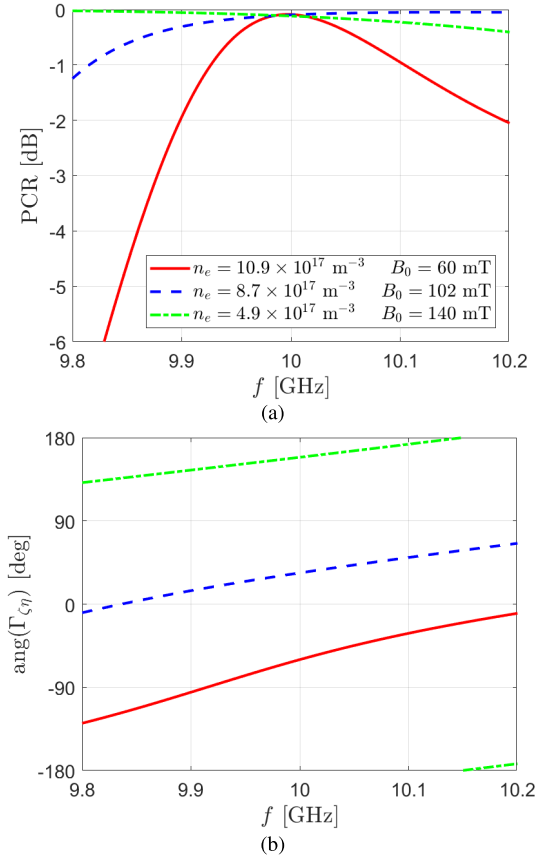

FIGURE 6. (a) Polarisation conversion ratio PCR, and (b) phase of the reflection coefficient $\Gamma_{\zeta\eta}$ in function of the operation frequency f. Three out of the eight states to implement beam-steering are analysed.

LP-to-CP conversion since AR $\leq$ 3. Moreover, $|\Gamma^+| > -1$ dB, namely a mild amount of power is dissipated on each plasma element due to Ohmic losses [39]. Thus, the reconfigurability of the reflected signal is ensured by relying on a discrete control of the plasma parameters [7]. Specifically, if n_e can be varied in the range 4.0×10^{17}-1.0×10^{18} m^{-3} and B_0 in the range 90-190 mT, it is possible to combine beam-steering and LP-to-CP conversion. These values are compatible with the technology at the state-of-the-art [31], [44]. It is worth noting that to ensure continuous control of the phase of the reflected wave (i.e., reconfigurability over 360°), B_0 shall span in a much larger range not compatible with the existing technology. Similarly, modifying z_{pl} is not much helpful since, reducing its size, both n_e and B_0 shall vary in a larger span to enable certain reconfigurability of the phase of the reflected wave [39]. Vice versa, if $z_{pl} > 0.8\lambda$ the phase of Γ^- is very sensitive to n_e [40]. Thus, it is not feasible to maintain a stable value of AR ≤ 3 accounting for uncertainty on n_e compatible with the technology at state of the art (between 10^{16} and 10^{17} m^{-3} [31]).

IV. FLOQUET ANALYSIS

The single plasma element is analysed numerically, accounting for practical constraints such as $L_{pl} \neq L$ [39]. This is propaedeutic to the design of plasma-based IRSs capable of combining beam-steering and polarization conversion. Specifically, both the elements intended for cross-polarisation and LP-to-CP conversion exhibit $L_{pl} = 12$ mm and $L = 15$ mm. The latter, corresponding to the lattice periodicity, equals 0.5λ at the operation frequency $f = 10$ GHz [39].

A. CROSS-POLARISATION CONVERSION

The plasma thickness is assumed $z_{pl} = 36$ mm, the collision frequency is $\nu = 3.1 \times 10^8$ Hz, the magnetostatic field is aligned along the ξ-axis (i.e., $\theta = 0°$), and the incident electric field is aligned along the η-axis. These values are consistent with the theoretical analysis reported in Section III-A.

The values of n_e-B_0 that maximize PCR are depicted in Fig. 5. The results associated with the current plasma element ($L_{pl} \neq L$) are compared against theoretical results ($L_{pl} = L$). Similar trends are obtained at the expense of a higher value of n_e, which is needed to enable the cross-polarization conversion. This is consistent with previous results [39], [40] highlighting that the presence of propagation paths outside the plasma medium has a detrimental effect on the performance of a plasma-based IRS. Notably, it is still possible to identify a continuous set of n_e-B_0 that enable cross-polarization

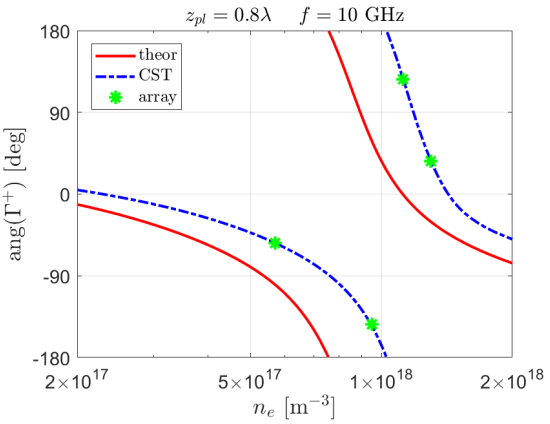

FIGURE 7. Phase of the reflection coefficient Γ^+ in function of the plasma density n_e. Theoretical ("theor") and Floquet ("CST") data were compared. Four configurations to implement LP-to-CP conversion maintaining a phase difference of ±90° are highlighted. $\theta = 90°$, $\nu = 3.1 \times 10^8$ Hz.

TABLE 3. States to implement LP-to-CP conversion maintaining a phase difference of ±90° according to the Floquet analysis (see Fig. 7).

n_e [10^{17} m^{-3}]	B_0 [mT]	ang(Γ^+) [deg]	$\lvert\Gamma^+\rvert$ [dB]	AR [dB]
13.0	110	36.1	−0.4	0.87
11.2	87	126.1	−0.5	0.11
9.5	104	−143.6	−0.3	0.50
5.7	190	−54.1	−0.1	0.79

conversion, the reconfigurability of the phase of $\Gamma_{\eta\zeta}$, and mild power losses (i.e., $|\Gamma_{\eta\zeta}| > -1$ dB). In Table 2, eight states are identified that present a relative phase shift of ±31.3° and maintain PCR > -0.2 dB. This is possible assuming n_e is reconfigurable in the range 4.9 × 10^{17}-1.1 × 10^{18} m^{-3} and B_0 in the range 60-140 mT, which is feasible with the actual technology [31], [44]. According to the array factor rule, a constant phase shift of ±31.3° enables a 10° beam-steering in a linear array [46]. This result has been exploited in Section V-A to design a plasma-based IRS that combines beam-steering and cross-polarization conversion.

In Fig. 6, the performance of three of the eight plasma states reported in Table 2 is analysed in the frequency range 9.8-10.2 GHz. The band in which PCR > -1 dB increases with B_0, the most critical configuration is the one in which $B_0 = 60$ mT where this condition is maintained in an interval of about 0.15 GHz. Similarly, the $B_0 = 60$ mT plasma state presents the largest phase variation over the considered frequency interval, which exceeds 90°.

B. LINEAR-TO-CIRCULAR CONVERSION

Consistently with the analysis reported in Section III-B, each plasma element has thickness $z_{pl} = 24$ mm, the collision frequency is $\nu = 3.1 \times 10^8$ Hz, the magnetostatic field is aligned along the ζ-axis (i.e., $\theta = 90°$), and the incident electric field has equal components along the η-axis and ζ-axis.

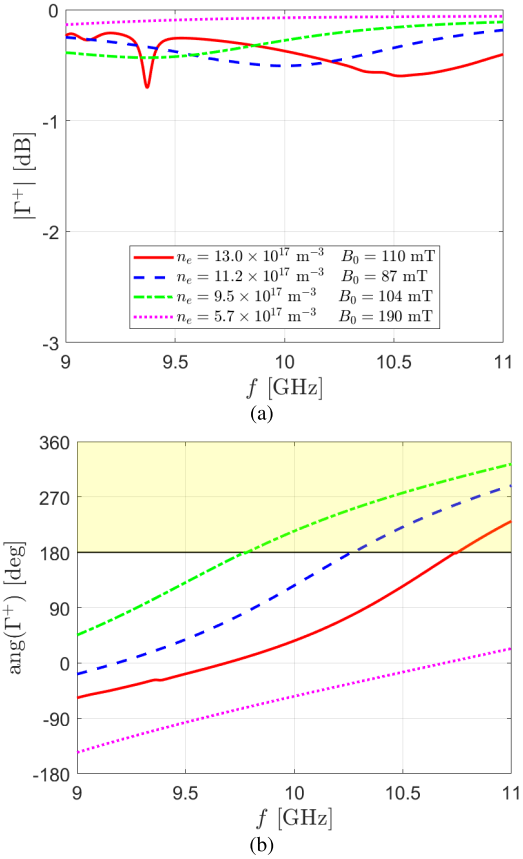

FIGURE 8. (a) Amplitude, and (b) phase of the reflection coefficient Γ^+ in function of the operation frequency f. The four configurations to implement LP-to-CP conversion maintaining a phase difference of ±90° are analysed. The yellow background indicates unwrapped values of the phase.

The phase of Γ^+ is depicted in Fig. 7 as a function of n_e. A comparison is performed between the considered plasma element and the theoretical results. Similar trends are obtained, but higher values of n_e are required if propagation paths outside the plasma medium occur [40]. This is not a significant issue provided that four states that present a phase difference of ±90° and ensure CP are feasible controlling n_e in the range 5.7 × 10^{17}-1.3 × 10^{18} m^{-3} and B_0 in the range 87-190 mT (see Table 3). In Fig. 8, the performance of these four plasma states is analysed in the frequency range 9-11 GHz. The reflection coefficient amplitude is maintained above −1 dB, confirming that Ohmic losses occurring within the plasma medium are very mild [39]. Regarding the reflection coefficient phase, no abrupt variation is registered in the frequency range of interest. Nonetheless, the phase difference between subsequent states decreases to ±40° at the edges of the frequency interval.

V. ARRAY DESIGN

A numerical analysis is performed to preliminary design plasma-based IRSs that enable beam-steering and polarization conversion. Two solutions, combining beam-steering

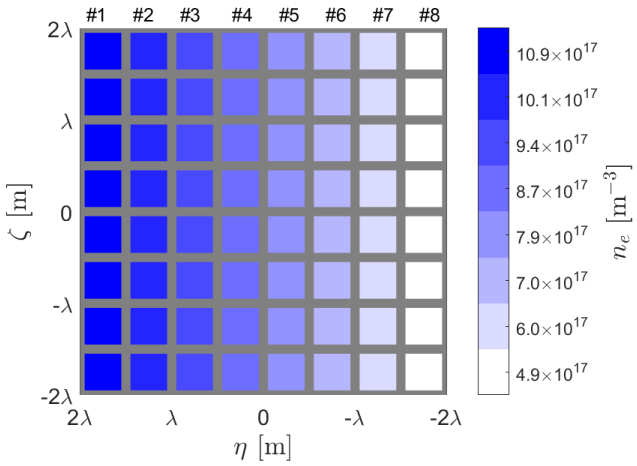

FIGURE 9. Plasma-based IRS to implement cross-polarization conversion and beam-steering. Each plasma element is colored according to the color scale and indicates the corresponding plasma density n_e. Numbering (#) refers to the columns of the array. Each element is characterized by $L = 15$ mm, $L_{pl} = 12$ mm, $z_{pl} = 36$ mm.

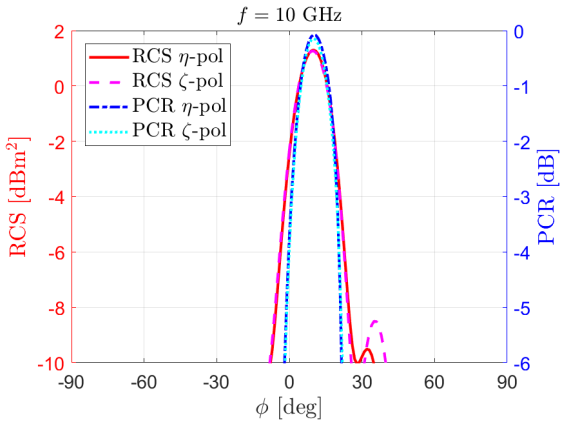

FIGURE 10. Polarization conversion ratio PCR and radar cross section RCS in function of the azimuth angle ϕ (ξ–η plane). Two polarization directions of the incident field are compared.

TABLE 4. Polarization conversion ratio PCR at $\phi = 10°$ for different operation frequencies f.

f [GHz]	9.6	9.7	9.8	9.9	10.0	10.1
PCR [dB]	−0.18	−0.10	−0.05	−0.06	−0.14	−0.34

TABLE 5. Performance parameters of the plasma-based IRS for different steering angles.

ϕ [deg]	PCR [dB]	SLL [dB]
0	−0.1	−14.8
10	−0.1	−9.8
20	−0.3	−5.5
30	−0.7	−4.4

with cross-polarization and LP-to-CP conversion, respectively, are presented.

A. CROSS POLARIZATION CONVERSION

The preliminary design of a plasma-based IRS that enables beam-steering and cross-polarization conversion relies on the plasma elements discussed in Section IV-A. The array envisions 8×8 plasma elements; the values of n_e displayed in Fig. 9 induce a 31.3° phase shift between adjacent columns which, according to the array factor rule, is associated to a 10° beam-steering in the ξ-η plane (see Table 2) [46]. Specifically, a linearly polarized plane wave propagating along the broadside direction $\phi = 0°$ is assumed to impinge the plasma-based IRS. Two cases have been analysed: incident wave polarized along the ζ-axis and the η-axis. It is worth noting that this corresponds to analyse the capability of the proposed design to steer the beam in azimuth and elevation, given that a 90° rotation of the polarization direction is equivalent to geometrically rotating the plasma-based IRS. The proposed design satisfies requirements for both beam-steering and cross-polarization conversion (see Fig. 10). At $f = 10$ GHz, the main lobe of the RCS occurs at $\phi = 10°$ with a relative side lobe level SLL of about -10 dB. Notably, PCR > -1 dB in an angle larger than 10° and centered on the direction of the main lobe. Moreover, power losses due to Ohmic effects are very mild, considering that 97% of the incident power is back-scattered. The proposed design is further analysed for different values of the operation frequency in Table 4. Despite the relatively narrow band in which all the eight plasma states maintain a constant phase difference and PCR > -1 dB (see Section IV-A), the performance of the plasma-based IRS satisfies requirements in the frequency range 9.6-10.1 GHz. Indeed, in this interval, the main lobe is registered in correspondence of $\phi = 10°$ and PCR > -0.4 dB.

The beam-steering capabilities of a plasma-based IRS have also been evaluated in terms of maximum steerable angle (see Table 5). Applying the array factor rule [46], plasma elements have been designed to ensure a certain steering angle and PCR > -1 dB. For a steering angle between 20° and 30°, the relative side lobe level (SLL) is modest. Larger values cannot rely on the array factor rule since the main lobe occurs in the broadside direction. This limitation is associated with the anisotropic back-scattering produced by plasma elements. Indeed, their RCS is maximum in the broadside direction and decreases by about -3 dB at $\phi = 40°$-45°. Thus a dedicated synthesis, which is out of the scope of the present work, would be needed to optimize the SLL and to extend the steering range up to a reasonable limit of 40°-45°.

B. LINEAR-TO-CIRCULAR CONVERSION

A plasma-based IRS that simultaneously enables beam-steering and LP-to-CP conversion has been preliminary designed. The array proposed is made of 8×8 elements

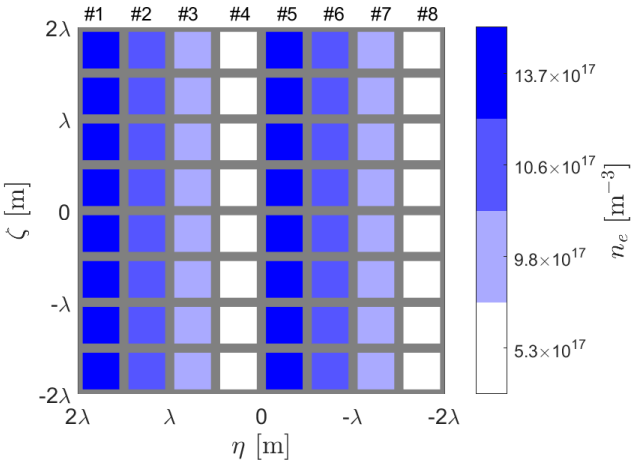

FIGURE 11. Plasma-based IRS to implement LP-to-CP conversion and beam-steering. Each plasma element is colored according to the color scale and indicates the corresponding plasma density n_e. Numbering (#) refers to the columns of the array. Each element is characterized by $L = 15$ mm, $L_{pl} = 12$ mm, $z_{pl} = 24$ mm.

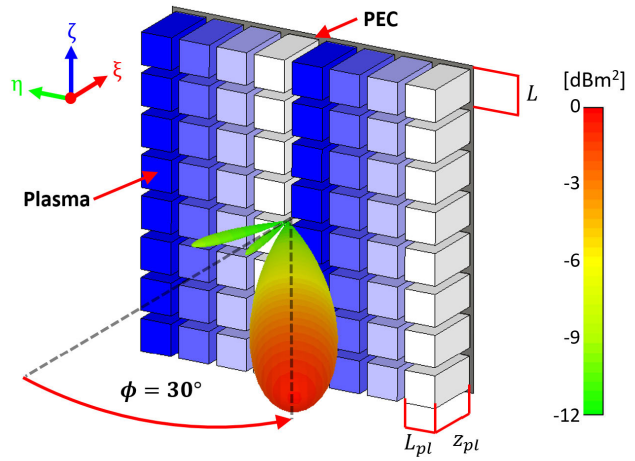

FIGURE 12. Polar plot of the radar cross section RCS referred to the plasma-based IRS depicted in Fig. 11 and assuming the optimized plasma states described in Table 6.

TABLE 6. Optimized plasma states to implement LP-to-CP conversion.

n_e [10^{17} m^{-3}]	B_0 [mT]	ang(Γ^+) [deg]	$\lvert\Gamma^+\rvert$ [dB]	AR [dB]
13.7	140	11.2	−0.3	5.35
10.6	108	164.2	−0.4	6.96
9.8	93	−159.9	−0.3	1.32
5.3	183	−47.1	−0.1	5.32

arranged in a rectangular lattice (see Fig. 11). The design is based on the discrete control of the plasma properties that envision four different states. Two configurations have been analysed; the first one assumes plasma properties that ensure a phase shift of 90° between adjacent columns (see Table 3); according to the array factor rule, this guarantees a 30°

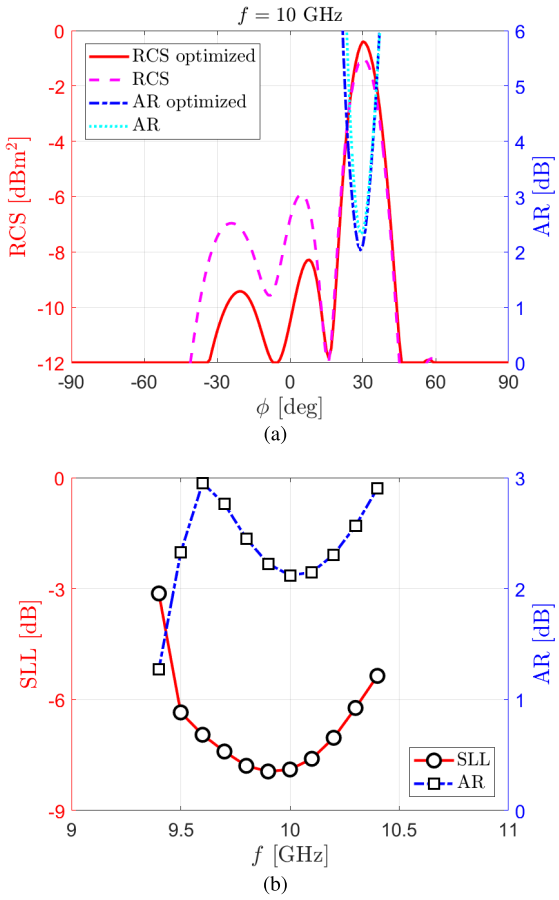

FIGURE 13. (a) Axial ratio AR and radar cross section RCS in function of the azimuth angle ϕ (ξ-η plane) assuming the plasma states described in Table 3 and the optimized ones reported in Table 6. (b) AR and relative side lobe level SLL in function of the operation frequency f for the optimized configuration.

steering of the reflected beam in the ξ-η plane [46]. In the second configuration, plasma properties are optimized to ensure a 30° steering while minimizing the relative SLL (see Table 6). The two solutions proposed match the requirements both in terms of beam-steering and LP-to-CP conversion at the operation frequency $f = 10$ GHz (see Fig. 12 and Fig. 13). Indeed, the main lobe, evaluated in terms of RCS, occurs in correspondence of $\phi = 30°$, and AR $\leq$ 3 dB in an interval of about 10° centered on this direction. A relative SLL of circa −5 dB is registered for the configuration based on the array factor rule, while it decreases at about −8 dB for the optimized one. The latter result is remarkable given that each plasma state does not guarantee AR $\leq$ 3 dB (see Table 6); as explained in Section V-A, this is related to the anisotropic radiation the plasma elements. The power back-scattered by the overall plasma-based IRS is 96% of the incident one, confirming that losses due to Ohmic effects are mild. For the optimized configuration, the operation bandwidth spans in the range 9.5-10.3 GHz assuming that an acceptable performance envisages: 1) main lobe in the direction $\phi = 30°$, 2) relative SLL $\leq$ 6 dB, 3) AR $\leq$ 3 dB in correspondence of the main lobe. It is worth remarking that, given the discrete control of

TABLE 7. Comparison between the proposed design (first line) and other plasma-based reflective surfaces previously discussed in the literature.

f [GHz]	polarization	steering	SLL [dB]	bandwidth [GHz]	ref.
10	**LP/CP**	**±30°**	**−8**	**0.5**	**-**
12	-	±30°	−15	2.0	[49]
10	CP	-	−12	2.5	[38]
10	-	±30°	−12	1.0	[39]
10	LP/CP	-	-	5.5	[40]

the plasma properties adopted for the LP-to-CP conversion, the concept of maximum steering angle is ill-defined since only specific diffraction patterns can be implemented [7]. To conclude, plasma-based IRSs are a feasible alternative to combine beam-steering and polarization conversion. Indeed, numerical results rely on plasma properties compatible with the technology at the state-of-the-art [31], [44].

C. DISCUSSION

Plasma-based IRSs that combine beam-steering and polarization control are compared against other numerical designs of plasma-based reflective surfaces proposed in the literature that operate in the GHz range (see Table 7). The solutions proposed in this paper are the only ones that combine beam-steering and polarization control. In [39] and [49], solutions to steer the reflected beam without any polarization control are proposed. Notably, the maximum steering angles presented are comparable to the values demonstrated in this work (i.e., about 30°), and the relative SLL is only a few dB lower. In [38] and [40] polarization converters are proposed, the first one [38] enables only LP-to-CP conversion while the second one [40] allows generic reconfigurability of the polarization state. Notably, the designs proposed in this work allow both cross-polarization and LP-to-CP conversion. Finally, the bandwidth of plasma-based solutions is relatively high, from 5% up to 50% of the central frequency.

VI. CONCLUSION AND FUTURE WORK

A feasibility study has been conducted to assess, for the first time, the use of plasma-based IRSs to combine beam-steering and polarization control in the GHz range. A theoretical model has been exploited to investigate both cross-polarization and LP-to-CP conversion. Moreover, the numerical design of two arrays that simultaneously enable 1) beam-steering and cross-polarization conversion, as well as 2) beam-steering and LP-to-CP, is presented. Both of these concepts are feasible assuming the plasma density is reconfigurable in the range 4.9×10^{17}-13.7×10^{17} m^{-3} and the magnetostatic field in the range 60-183 mT. These values are consistent with the plasma technology at the state-of-the-art [31], [44]. Moreover, both concepts present a bandwidth between 0.5-0.8 GHz. Thus, plasma-based IRS is proven to be an extremely appealing technology in terms of multifunctionality.

Even though the proposed design is feasible, a few challenges shall be faced before realizing a proof-of-concept of this technology. First, the solutions implemented for the electronics dedicated to plasma production are usually bulky and power-consuming [30]. With this regard, it is possible to take advantage of the technological advances in space propulsion, where miniaturized solutions are available [50], [51]. Second, plasma discharges shall be controlled via an "intelligent" algorithm. Also, in this case, a partial solution can be derived from the plasma display panels application where strategies to control the ignition of multiple plasma elements are available [52]. Third, plasma sources employed in the field of GPAs usually have a cylindrical shape [35]. To implement the design proposed in this work, it is necessary to develop square plasma blocks. Nonetheless, the literature is plenty of rectangular dielectric barrier discharges (DBD) [52] that have been developed, for example, in the field of plasma display panels. A practical implementation might envision a segmented metallic plate in which ground high-voltage electrodes are integrated. This is not expected to interfere with the signal [35] given that the power to ignite DBDs is usually provided in the MHz range [52]. Thus, the realization and test of a prototype plasma-based IRS will be the subject of future work.

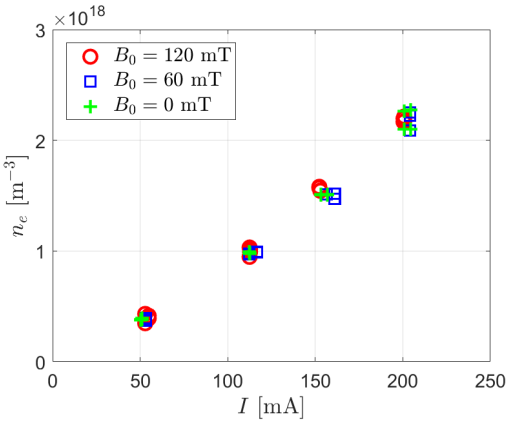

FIGURE 14. Measured plasma density n_e in function of the discharge current I for three different values of the magnetostatic field B_0.

APPENDIX A PLASMA MEASURES

Plasma discharges usually employed in GPAs [30], [47], [48] have been realized and tested to evaluate further the feasibility of the IRSs proposed in this work. Plasma is produced by applying a sufficiently high voltage (100 V range [35]) between two electrodes placed at the opposite ends of a glass vessel that contains argon gas. The plasma density n_e has been evaluated via interferometric measures [53] for different values of the discharge current I and the magnetostatic field B_0 (see Fig. 14). The former is provided and monitored via a custom-built power processing unit (PPU), and the latter is generated via electromagnets. Notably, there is a linear correlation between n_e and I while B_0 has a negligible effect

on the achievable plasma density [28], [29]. Thus, the two variables that determine the behavior of a plasma-based IRS (i.e., n_e and B_0) can be controlled independently. Moreover, experiments show that the values of n_e assumed for the numerical design are perfectly feasible as the possibility to vary B_0 in an interval of 120 mT.

REFERENCES

[1] Q. Wu, S. Zhang, B. Zheng, C. You, and R. Zhang, "Intelligent reflecting surface-aided wireless communications: A tutorial," *IEEE Trans. Commun.*, vol. 69, no. 5, pp. 3313–3351, May 2021.

[2] E. Basar, M. Di Renzo, J. De Rosny, M. Debbah, M.-S. Alouini, and R. Zhang, "Wireless communications through reconfigurable intelligent surfaces," *IEEE Access*, vol. 7, pp. 116753–116773, 2019.

[3] Q. Wu and R. Zhang, "Towards smart and reconfigurable environment: Intelligent reflecting surface aided wireless network," *IEEE Commun. Mag.*, vol. 58, no. 1, pp. 106–112, Nov. 2019.

[4] V. Tapio, I. Hemadeh, A. Mourad, A. Shojaeifard, and M. Juntti, "Survey on reconfigurable intelligent surfaces below 10 GHz," *EURASIP J. Wireless Commun. Netw.*, vol. 2021, no. 1, Dec. 2021, Art. no. 175.

[5] J. Rodriguez-Zamudio, J. I. Martinez-Lopez, J. Rodriguez-Cuevas, and A. E. Martynyuk, "Reconfigurable reflectarrays based on optimized spiraphase-type elements," *IEEE Trans. Antennas Propag.*, vol. 60, no. 4, pp. 1821–1830, Apr. 2012.

[6] S. Hu, F. Rusek, and O. Edfors, "Beyond massive MIMO: The potential of positioning with large intelligent surfaces," *IEEE Trans. Signal Process.*, vol. 66, no. 7, pp. 1761–1774, Apr. 2018.

[7] T. J. Cui, M. Q. Qi, X. Wan, J. Zhao, and Q. Cheng, "Coding metamaterials, digital metamaterials and programmable metamaterials," *Light, Sci. Appl.*, vol. 3, no. 10, Oct. 2014, Art. no. 218.

[8] S. A. Khaleel, E. K. I. Hamad, N. O. Parchin, and M. B. Saleh, "Programmable beam-steering capabilities based on graphene plasmonic THz MIMO antenna via reconfigurable intelligent surfaces (RIS) for IoT applications," *Electronics*, vol. 12, no. 1, Dec. 2022, Art. no. 164.

[9] M. B. Heydari, M. Karimipour, and M. M. Shirkolaei, "Analytical study of highly adjustable plasmonic modes in graphene-based heterostructure for THz applications," *J. Opt.*, pp. 1–7 Jan. 2023, doi: 10.1007/s12596-022-01084-8.

[10] M. M. Shirkolaei and J. Ghalibafan, "Magnetically scannable slotted waveguide antenna based on the ferrite with gain enhancement," *Waves Random Complex Media*, pp. 1–11, Oct. 2021, doi: 10.1080/17455030.2021.1983234.

[11] C. Huang, W. Pan, X. Ma, B. Zhao, J. Cui, and X. Luo, "Using reconfigurable transmitarray to achieve beam-steering and polarization manipulation applications," *IEEE Trans. Antennas Propag.*, vol. 63, no. 11, pp. 4801–4810, Nov. 2015.

[12] Z. Wu, L. Li, Y. Li, and X. Chen, "Metasurface superstrate antenna with wideband circular polarization for satellite communication application," *IEEE Antennas Wireless Propag. Lett.*, vol. 15, pp. 374–377, 2016.

[13] Y. Deng, C. Wu, C. Meng, S. I. Bozhevolnyi, and F. Ding, "Functional metasurface quarter-wave plates for simultaneous polarization conversion and beam steering," *ACS Nano*, vol. 15, no. 11, pp. 18532–18540, Nov. 2021.

[14] H. Yang, X. Cao, F. Yang, J. Gao, S. Xu, M. Li, X. Chen, Y. Zhao, Y. Zheng, and S. Li, "A programmable metasurface with dynamic polarization, scattering and focusing control," *Sci. Rep.*, vol. 6, pp. 1–11, Oct. 2016.

[15] I.-G. Lee, J.-Y. Kim, and I.-P. Hong, "Design of multi-functional transmitarray with active linear polarization conversion and beam steering capabilities," *Appl. Sci.*, vol. 12, no. 9, Apr. 2022, Art. no. 4319.

[16] M. Hwang, G. Kim, J. Kim, and S. Kim, "A simultaneous beam steering and polarization converting S-band transmitarray antenna," *IEEE Access*, vol. 10, pp. 105111–105119, 2022.

[17] L. D. Palma, A. Clemente, L. Dussopt, R. Sauleau, P. Potier, and P. Pouliguen, "Circularly-polarized reconfigurable transmitarray in Ka-band with beam scanning and polarization switching capabilities," *IEEE Trans. Antennas Propag.*, vol. 65, no. 2, pp. 529–540, Feb. 2017.

[18] A. Safaripour, S. M. Bowers, K. Dasgupta, and A. Hajimiri, "Dynamic polarization control of two-dimensional integrated phased arrays," *IEEE Trans. Microw. Theory Techn.*, vol. 64, no. 4, pp. 1066–1077, Apr. 2016.

[19] M. H. Dahri, M. H. Jamaluddin, M. Khalily, M. I. Abbasi, R. Selvaraju, and M. R. Kamarudin, "Polarization diversity and adaptive beamsteering for 5G reflectarrays: A review," *IEEE Access*, vol. 6, pp. 19451–19464, 2018.

[20] B. Liu, J. Du, X. Jiang, Y. Li, S. Wong, Q. Cheng, T. J. Cui, and Q. Zhang, "All-in-one integrated multifunctional broadband metasurface for analogue signal processing, polarization conversion, beam manipulation, and near-field sensing," *Adv. Opt. Mater.*, vol. 10, no. 20, Oct. 2022, Art. no. 2201217.

[21] Y. Jing, Y. Li, J. Zhang, J. Wang, M. Feng, T. Qiu, H. Wang, Y. Han, H. Ma, and S. Qu, "Achieving circular-to-linear polarization conversion and beam deflection simultaneously using anisotropic coding metasurfaces," *Sci. Rep.*, vol. 9, no. 1, pp. 1–8, Aug. 2019.

[22] L. Guo, P. K. Tan, and T. H. Chio, "A simple approach to achieve polarization diversity in broadband reflectarrays using single-layered rectangular patch elements," *Microw. Opt. Technol. Lett.*, vol. 57, no. 2, pp. 305–310, Feb. 2015.

[23] M. A. Joyal, R. E. Hani, M. Riel, Y. Demers, and J. J. Laurin, "A reflectarray-based dual-surface reflector working in circular polarization," *IEEE Trans. Antennas Propag.*, vol. 63, no. 4, pp. 1306–1313, Apr. 2015.

[24] T. Anderson, *Plasma Antennas*. Norwood, MA, USA: Artech House, 2020.

[25] J. P. Rayner, A. P. Whichello, and A. D. Cheetham, "Physical characteristics of plasma antennas," *IEEE Trans. Plasma Sci.*, vol. 32, no. 1, pp. 269–281, Feb. 2004.

[26] G. Borg, J. Harris, N. Martin, D. Thorncraft, R. Milliken, D. Miljak, B. Kwan, T. Ng, and J. Kircher, "Plasmas as antennas: Theory, experiment and applications," *Phys. Plasmas*, vol. 7, no. 5, pp. 2198–2202, May 2000.

[27] T. Naito, S. Yamaura, Y. Fukuma, and O. Sakai, "Radiation characteristics of input power from surface wave sustained plasma antenna," *Phys. Plasmas*, vol. 23, no. 9, Sep. 2016, Art. no. 093504.

[28] N. Souhair, M. Magarotto, E. Majorana, F. Ponti, and D. Pavarin, "Development of a lumping methodology for the analysis of the excited states in plasma discharges operated with argon, neon, krypton, and xenon," *Phys. Plasmas*, vol. 28, no. 9, Sep. 2021, Art. no. 093504.

[29] M. Guaita, M. Magarotto, M. Manente, D. Pavarin, and M. Lavagna, "Semi-analytical model of a helicon plasma thruster," *IEEE Trans. Plasma Sci.*, vol. 50, no. 2, pp. 425–438, Feb. 2022.

[30] P. De Carlo, M. Magarotto, G. Mansutti, S. Boscolo, A.-D. Capobianco, and D. Pavarin, "Experimental characterization of a plasma dipole in the UHF band," *IEEE Antennas Wireless Propag. Lett.*, vol. 20, no. 9, pp. 1621–1625, Sep. 2021.

[31] A. Daykin-Iliopoulos, F. Bosi, F. Coccaro, M. Magarotto, A. Papadimopoulos, P. De Carlo, C. Dobranszki, I. Golosnoy, and S. Gabriel, "Characterisation of a thermionic plasma source apparatus for high-density gaseous plasma antenna applications," *Plasma Sources Sci. Technol.*, vol. 29, no. 11, Nov. 2020, Art. no. 115002.

[32] G. Mansutti, P. De Carlo, M. A. Hannan, F. Boulos, P. Rocca, A.-D. Capobianco, M. Magarotto, and A. Tuozzi, "Modeling and design of a plasma-based transmit-array with beam scanning capabilities," *Results Phys.*, vol. 16, Mar. 2020, Art. no. 102923.

[33] G. Mansutti, P. De Carlo, M. Magarotto, M. A. Hannan, P. Rocca, A.-D. Capobianco, D. Pavarin, and A. Tuozzi, "Design of a hybrid metal-plasma transmit-array with beam-scanning capabilities," *IEEE Trans. Plasma Sci.*, vol. 50, no. 3, pp. 662–669, Mar. 2022.

[34] M. Magarotto, P. de Carlo, G. Mansutti, F. J. Bosi, N. E. Buris, A.-D. Capobianco, and D. Pavarin, "Numerical suite for gaseous plasma antennas simulation," *IEEE Trans. Plasma Sci.*, vol. 49, no. 1, pp. 285–297, Jan. 2021.

[35] P. De Carlo, M. Magarotto, G. Mansutti, A. Selmo, A.-D. Capobianco, and D. Pavarin, "Feasibility study of a novel class of plasma antennas for SatCom navigation systems," *Acta Astronautica*, vol. 178, pp. 846–853, Jan. 2021.

[36] H. A. E.-A. Malhat and A. S. Zainud-Deen, "Dual/circular polarization beam shaping of time-modulated plasma-based magneto-electric dipole antenna arrays," *Opt. Quantum Electron.*, vol. 54, no. 2, Feb. 2022, Art. no. 111.

[37] S. H. Zainud-Deen, M. M. Badawy, and H. A. E.-A. Malhat, "Dielectric resonator antenna loaded with reconfigurable plasma metamaterial polarization converter," *Plasmonics*, vol. 14, no. 6, pp. 1321–1328, Dec. 2019.

[38] H. A. E.-A. Malhat and S. H. Zainud-Deen, "Plasma-based artificial magnetic conductor for polarization reconfigurable dielectric resonator antenna," *Plasmonics*, vol. 15, no. 6, pp. 1913–1924, Dec. 2020.

[39] M. Magarotto, L. Schenato, P. De Carlo, and A.-D. Capobianco, "Feasibility of a plasma-based intelligent reflective surface," *IEEE Access*, vol. 10, pp. 97995–98003, 2022.

[40] M. Magarotto, L. Schenato, P. De Carlo, and A.-D. Capobianco, "Plasma-based reflective surface for polarization conversion," *IEEE Trans. Antennas Propag.*, vol. 71, no. 3, pp. 2849–2854, Mar. 2023, doi: 10.1109/TAP.2023.3239165.
[41] L. Zhang, X. Q. Chen, S. Liu, Q. Zhang, J. Zhao, J. Y. Dai, G. D. Bai, X. Wan, Q. Cheng, G. Castaldi, and V. Galdi, "Space-time-coding digital metasurfaces," *Nature Commun.*, vol. 9, no. 1, 2018, Art. no. 4334.
[42] Y. Zhou, G. Zhang, H. Chen, P. Zhou, X. Wang, L. Zhang, L. Zhang, J. Xie, and L. Deng, "Design of phase gradient coding metasurfaces for broadband wave modulating," *Sci. Rep.*, vol. 8, no. 1, Jun. 2018, Art. no. 8672.
[43] A. Slalmi, H. Chaibi, A. Chehri, R. Saadane, and G. Jeon, "Toward 6G: Understanding network requirements and key performance indicators," *Trans. Emerg. Telecommun. Technol.*, vol. 32, no. 3, Mar. 2021, Art. no. e4201.
[44] K. Takahashi, "Magnetic nozzle radiofrequency plasma thruster approaching twenty percent thruster efficiency," *Sci. Rep.*, vol. 11, no. 1, Feb. 2021, Art. no. 2768.
[45] J. A. Bittencourt, *Fundamentals of Plasma Physics*. Berlin, Germany: Springer, 2004.
[46] C. A. Balanis, *Antenna Theory: Analysis and Design*. Hoboken, NJ, USA: Wiley, 2015.
[47] M. Magarotto, L. Schenato, P. De Carlo, M. Santagiustina, A. Galtarossa, and A.-D. Capobianco, "Design of a plasma-based intelligent reflecting surface," *Phys. Plasmas*, vol. 30, no. 4, Apr. 2023, Art. no. 043509.
[48] M. Magarotto, P. De Carlo, L. Schenato, M. Santagiustina, A. Galtarossa, D. Pavarin, and A.-D. Capobianco, "Feasibility study on a plasma based reflective surface for SatCom systems," *Acta Astronautica*, vol. 208, pp. 55–61, Jul. 2023.
[49] S. H. Zainud-Deen, H. A. Malhat, S. M. Gaber, M. Ibrahim, and K. H. Awadalla, "Plasma reflectarrays," *Plasmonics*, vol. 8, no. 3, pp. 1469–1475, Sep. 2013.
[50] M. Manente, F. Trezzolani, M. Magarotto, E. Fantino, A. Selmo, N. Bellomo, E. Toson, and D. Pavarin, "REGULUS: A propulsion platform to boost small satellite missions," *Acta Astronautica*, vol. 157, pp. 241–249, Apr. 2019.
[51] N. Bellomo, M. Magarotto, M. Manente, F. Trezzolani, R. Mantellato, L. Cappellini, D. Paulon, A. Selmo, D. Scalzi, M. Minute, and M. Duzzi, "Design and in-orbit demonstration of REGULUS, an iodine electric propulsion system," *CEAS Space J.*, vol. 14, no. 1, pp. 79–90, Jan. 2022.
[52] J. P. Boeuf, "Plasma display panels: Physics, recent developments and key issues," *J. Phys. D, Appl. Phys.*, vol. 36, no. 6, pp. R53–R79, Mar. 2003.
[53] O. Tudisco, A. L. Fabris, C. Falcetta, L. Accatino, R. De Angelis, M. Manente, F. Ferri, M. Florean, C. Neri, C. Mazzotta, D. Pavarin, F. Pollastrone, G. Rocchi, A. Selmo, L. Tasinato, F. Trezzolani, and A. A. Tuccillo, "A microwave interferometer for small and tenuous plasma density measurements," *Rev. Sci. Instrum.*, vol. 84, no. 3, Mar. 2013, Art. no. 033505.

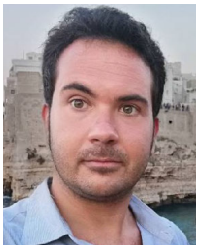

MIRKO MAGAROTTO (Member, IEEE) received the M.Sc. degree in aerospace engineering and the Ph.D. degree in science technology and measurements for space from the University of Padua, Padua, Italy, in 2015 and 2019, respectively. He is currently a Research Fellow (RTDa) with the Department of Information Engineering, University of Padua. His current research interests include plasma antennas, plasma numerical simulation, and electric space propulsion.

LUCA SCHENATO (Member, IEEE) received the M.Sc. degree in telecommunication engineering and the Ph.D. degree in electronic and telecommunication engineering from the University of Padua, Padua, Italy, in 2003 and 2007, respectively. He is currently an Assistant Professor (RTDb) with the Department of Information Engineering, University of Padua. His research interests include optical fiber sensors, optical fiber-based devices, and intelligent reflective surfaces.

MARCO SANTAGIUSTINA (Member, IEEE) received the M.Sc. degree in electronic engineering and the Ph.D. degree in electronic and telecommunication engineering from the University of Padua, Padua, Italy, in 1992 and 1996, respectively. He is currently a Full Professor with the Department of Information Engineering, University of Padua. His current research interests include nonlinear optics, optical fibers, and electromagnetic field theory.

ANDREA GALTAROSSA (Fellow, IEEE) is currently a Full Professor of electromagnetic waves and photonics with the Department of Information Engineering, University of Padua, Italy. He has coauthored more than 200 papers in journals and conference proceedings. His research interests include optical fiber designs, the distributed characterization of single mode and special fibers, and distributed sensing. He has been a member of the Technical Program Committee for the European Conference on Optical Communication (ECOC) and the Optical Fiber Communication Conference (OFC). He is a fellow of OPTICA. He has been the Topical Editor and the Deputy Editor of *Optics Letters*.

ANTONIO-DANIELE CAPOBIANCO (Member, IEEE) received the M.Sc. degree in electronic engineering and the Ph.D. degree in electronic and telecommunication engineering from the University of Padua, Padua, Italy, in 1989 and 1994, respectively. He is an Associate Professor with the Department of Information Engineering, University of Padua. His current research interests include theory and numerical modeling in photonics, plasmonics, and microwave antennas.

Open Access funding provided by 'Università degli Studi di Padova' within the CRUI CARE Agreement